Photometric and spectroscopic study of the young open cluster NGC 1893

Amparo Marco and Guillermo Bernabeu

Dpto. de Física, Ingeniería de Sistemas y Teoría de la Señal, Universidad de Alicante,

Apdo. de Correos 99, E-03080, Alicante, Spain

amparo@astronomia.disc.ua.es

and

Ignacio Negueruela[1]

Observatoire de Strasbourg, 11 rue de l'Université, F67000 Strasbourg, France

SAX SDC, ASI, c/o Nuova Telespazio, via Corcolle 19, I00131 Rome, Italy

Received _____; accepted _____

[1]Guest investigator of the UK Astronomy Data Centre

ABSTRACT

We present $uvby\beta$ CCD photometry of the field of the open cluster NGC 1893. Our photometry is deep enough to cover the complete main sequence B spectral type. We identify $\sim$ 50 very likely members of the cluster down to spectral type B9-A0, some of which have much higher reddenings than the average. We derive a color excess $E(b-y) = 0.33 \pm 0.03$ and a dereddened distance modulus $V_0 - M_V = 13.9 \pm 0.2$. From the β index, we identify several candidates as emission-line stars, for which we have obtained spectroscopy. Three of them display spectra corresponding to spectral type F, but showing Hα in emission. Photometric measurements in this and previous studies indicate strong variability. These characteristics show them to be pre-main-sequence stars of spectral type F. We also identify two likely Herbig Be stars. These results hint at the existence of a sizable pre-main-sequence population in NGC 1893.

Subject headings: techniques:photometry – Galaxy:open clusters and associations:individual:NGC 1893 – stars: evolution – emission-line, Be – formation – pre-main-sequence

1. Introduction

NGC 1893 is a very young cluster immersed in the bright diffuse nebulosity IC 410, associated with two pennant nebulae, Shain and Gaze 129 and 130, and obscured by several conspicuous dust clouds. UBV photometry of NGC 1893 has been presented by Hoag et al. (1961), Cuffey (1973) and Massey et al. (1995). Tapia et al. (1991, henceforth T91) performed near-infrared and Strömgren photometry for 47 stars in the field of the cluster. They estimate the age of the cluster to be 4×10^6 yr, derive a distance

modulus $(M-m)_0 = 13.18 \pm 0.11$, and an extinction to the cluster $A_V = 1.68$. Strömgren photometry for 50 stars in the field of NGC 1893 has also been reported by Fitzsimmons (1993), who confirms the distance and age found by T91. Vallenari et al. (1999) performed near-infrared photometry of the cluster and came to the conclusion that there could be many pre-main-sequence candidates in NGC 1893, though their method did not allow clear discrimination from field interlopers.

Even though the earliest spectral type stars in NGC 1893 are rather bright, spectroscopic work on cluster members is very scarce. Massey et al. (1995) obtained intermediate-resolution spectra of a few of the brightest stars in the cluster and derived their spectral classification. Rolleston et al. (1993) obtained higher resolution spectroscopy of eight stars whose photometric indices were consistent with an early B-type spectral classification and derived their astrophysical parameters and metal abundances.

This paper belongs to a series dedicated to the study of the B-star population of young Galactic open clusters. We use the photometric system $uvby\mathrm{H}\beta$ because it is the most adequate for the study of early-type stars, since it has been purposely designed to provide accurate measurements of their intrinsic properties. After identifying a large number of a likely B-type members, we have carried out a spectroscopic study of some stars showing interesting peculiarities.

2. Observations

2.1. Photometry

The data were obtained with the Jacobus Kapteyn Telescope (JKT), located at the Observatorio del Roque de los Muchachos, La Palma, Spain, in December 1997, using the 1024 x 1024 TEK 4 chip CCD and the four Strömgren $uvby$ and the narrow and wide Hβ

filters. Pixel size was 0.″331 in such a way that the whole field covered by each frame was 5.′6 x 5.′6. Four frames covering the whole of the central core of the cluster were taken (central coordinates are displayed in Table 1). Figures 1(a)-1(d) show plots of the observed fields. The dot sizes are indicative of the relative instrumental y magnitude. Each field was observed twice using different exposure times, so that the widest range of magnitudes possible was observed with good signal-to-noise ratio.

Throughout this paper the nomenclature used will be that of Cuffey (1973), where the whole cluster area was divided into smaller zones, using three rings and four sectors. Designation of a star is given by stating the sector, the ring, and the number of the star in that particular zone. For two stars that were not observed by Cuffey, a new nomenclature has been adopted, designating them by listing their number after a prefix "s5"(s5000 and s5001).

The reduction of all frames was done with the IRAF routines for the bias and flat-field corrections. The photometry has been obtained by PSF-fitting using the DAOPHOT package (Stetson 1987) provided by IRAF. In order to construct the PSF empirically, we manually select bright stars in the least-crowded areas (typically 7−12 in each frame) trying to cover the largest possible magnitude interval in each frame (typically an interval of 4-5 instrumental magnitudes). We preferentially choose stars with no or very few close neighbours as PSF stars, since this results in a simpler and faster process. Once we have the list of PSF stars, we determine an initial PSF by fitting Gaussian functions. Afterwards, we run the PSF-fitting photometry routine NSTAR, which fits PSF's to all the groups (PSF star + neighbors) in a frame simultaneously. Most of these groups contain only the PSF star. When a PSF star has neighbors, we previously check that the FIT radii ($\approx$ FWHM) of the neighbor stars do not merge into the PSF radius of the PSF star, so that we can apply the procedure without modifying any parameters. The routine SUBSTAR is then used

to subtract the PSF stars and their neighbors from the frames. We examine the subtracted image and make sure that they have been cleaned completely. Examination shows that there is no systematic pattern of PSF variability with position on the chip, and therefore the PSF is constant across the frame. Finally we run the routine ALLSTAR and obtain the instrumental magnitudes from all stars in each frame. Since our standard stars were selected from other program clusters in the same campaign and the aperture size used was the same in all campaign frames (12 pixels), no aperture correction is necessary. The atmospheric extinction corrections were performed using the RANBO2 program, which implements the method described by Manfroid (1993). It has been shown the choice of standard stars for the transformation is a critical issue in $uvby\beta$ photometry. Transformations made only with unreddened stars introduce large systematic errors when applied to reddened stars, even if the color range of the standards brackets that of the program stars (Manfroid & Sterken, 1987 and Crawford, 1994). Our data cover a very wide range of spectral types with a correspondingly wide range of intrinsic colors. Moreover, during this campaign several clusters with different interstellar reddenings were observed.

A preliminary list of standard stars was built by selecting a number of putatively non-variable non-peculiar stars in the clusters h and χ Persei, NGC 2169, NGC 6910 and NGC 1039, which had been observed with the same Kitt Peak telescopes and instrumentation used to define the $uvby$ Crawford & Barnes (1970b) and Hβ Crawford & Mander (1966) standard systems, so that there is no doubt that the photometric values are in the standard systems. Since the original h and χ Persei observations (Crawford et al. 1970) do not include V values, we used values given by Johnson & Morgan (1955), which were also taken with the same instrumentation, for the V transformation. The list of standard stars used can be found in Table 2 along with their standard values, used for the transformation, taken from Crawford et al. (1970) and Johnson & Morgan (1955) for h and χ Persei, Perry et al. (1978) for NGC 2169, Crawford et al. (1977) for NGC 6910 and

Canterna et al. (1979) for NGC 1039. Spectral types, when available, have been taken from Schild (1965) and Slettebak (1968) for h and χ Persei, Perry et al. (1978) for NGC 2169, Morgan & Harris (1956) and Hoag & Applequist (1965) for NGC 6910 and Canterna et al. (1979) for NGC 1039.

With the extinction corrected magnitudes, the following $uvby$ transformation is obtained using the equations from Crawford and Barnes (1970b), where the coefficients have been computed following the procedure described in detail by Grønbech et al.(1976) using the selected standard stars list:

$$V = 11.269 \quad + 0.091(b-y) \; + \; y_{\rm i} \tag{1}$$
$$\pm\, 0.003 \quad \pm\, 0.007$$

$$(b-y) = 0.636 \quad + 1.070(b-y)_{\rm i} \tag{2}$$
$$\pm\, 0.008 \quad \pm\, 0.008$$

$$m_1 = \; -\, 0.523 + 1.009 m_{1\rm i} - 0.206(b-y) \tag{3}$$
$$\pm\, 0.008 \quad \pm\, 0.015 \quad \pm\, 0.009$$

$$c_1 = 0.543 \quad + 1.019 c_{1\rm i} \; + 0.257(b-y) \tag{4}$$
$$\pm\, 0.004 \quad \pm\, 0.004 \quad \pm\, 0.007$$

where the subindex "i" stands for instrumental magnitudes.

The transformed values for the 41 standard stars used is given in Table 3, together with their precision and their deviation with respect to the cataloged standard values. Table 4 shows the mean catalog minus transformed values for the standard stars and their standard deviations, which constitute a measure of the accuracy of the transformation. From the

mean differences between catalog and transformed values, it is clear that there is not a significant offset between our photometry and the standard system. Since the individual differences for a few stars seem to be rather high, an attempt was made to improve the transformation by removing these stars from the standard list, but it was found that the transformation coefficients and their precision did not improve.

The Hβ instrumental system and transformation equations were computed following the procedure described in detail by Crawford & Mander (1966). The transformation coefficients are $a = 3.514$ and $b = 1.059$. Transformed values and their differences with respect to mean catalog values are given in Table 3. The mean difference is -0.003 with a standard deviation 0.031, which, as in the case of the *uvby* transformation, indicates that there is no significant offset with respect to the standard system.

2.2. Spectroscopy

Spectroscopy of selected stars was taken on February 3 – 6, 2000, using the 1.52-m G. D. Cassini telescope, at the Loiano Observatory, Italy, equipped with the Bologna Faint Object Spectrograph and Camera (BFOSC). The detector was a 2048 x 2048 Loral CCD with a 15μm pixel size, which covers a 15.′1 x 15.′1 field. Due to the sky conditions, only low-resolution spectroscopy could be performed for stars with $V > 14$. We used BFOSC grism#4, which gives a resolution of 220 Å/mm over the 4700 – 8800 Å interval (the resolution element is ~ 8.3Å). With this configuration, a 30-min exposure on one of the fainter ($V \approx 15$) targets gave typically a Signal-to-Noise ratio per pixel in the wavelength direction (integrated over all columns) of ~ 70 on the red continuum. For brighter stars, we also took spectra using BFOSC grism#3, which gives 170 Å/mm over the blue part of the spectrum (resolution ~ 5.5Å). A log of the observations is presented in Table 5.

In addition, we have retrieved from the ING Archive all the observations used in the work of Rolleston et al. (1993), in order to derive spectral types for those stars by comparing them to spectra of MK standard stars observed at a similar resolution by Steele et al. (1999). Details for these data can be found in Rolleston et al. (1993).

All the data have been reduced following the standard procedure by using the *Starlink* software packages CCDPACK (Draper, 1998) and FIGARO (Shortridge et al., 1997) and analysed using FIGARO and DIPSO (Howarth et al., 1997).

3. Results

3.1. Photometry

We have obtained $ubvy\beta$ CCD photometry for 111 stars, reaching a magnitude limit $V \approx 15.9$. In Table 6 we present the resulting values for $V, (b-y), m_1, c_1$ and β, together with the number of observations for each star and their pixel coordinates in the corresponding frame (when a star is present in more than one field, we give its coordinates in the frame in which it is better centered).

3.2. Member Stars and Reddening Slopes

The first step in the analysis is the estimate of membership for the stars measured in each field. Since previous authors have already shown that NGC 1893 is a young cluster in which B-type stars have not had time to leave the main sequence (T91) and our magnitude limit implies that cluster members can only be seen up to an absolute magnitude $M_V \approx +1$, all the cluster members in our sample must be OB stars. Therefore we can calculate the free reddening indices $[m_1]$, $[c_1]$ and $[u-b]$, where

$$[m_1] = m_1 + 0.32(b-y) \tag{5}$$

$$[c_1] = c_1 - 0.20(b-y) \tag{6}$$

$$[u-b] = [c_1] + 2[m_1] \tag{7}$$

and then use the $[c_1]$ – $[m_1]$ and β – $[u-b]$ diagrams for the approximate spectral classification of cluster stars.

Figure 2 shows the $[c_1]$ – $[m_1]$ diagram for all observed stars. As already noted by T91, most members of NGC 1893 lie to the right of the average intrinsic color loci of field main sequence stars (determined using the standard relations from Perry et al. 1987). All the stars lying close to the B-type line in the $[c_1]$ – $[m_1]$ diagram fall along a narrow strip in the β – $[u-b]$ diagram, which we interpret as the cluster main sequence (see Figure 3).

The only exceptions are S3R1N3, which is an emission line star (see below) and S3R1N4, which also has a much lower β index than expected. Spectroscopy of this object will be necessary in order to establish whether it is a Be star or an evolved star (since its position in the $V - c_1$ diagram makes unlikely its being a non-member). The three stars in our sample previously classified (spectroscopically) as O-type members fall along the main sequence as well. The validity of the $[u-b]$ index as an approximate spectral classification indicator can be checked by comparing the values obtained with the spectral types derived spectroscopically (Table 7).

From the β – $[u-b]$ diagram, we have selected all those stars falling along the B-star strip, those on the border area between B9 and A0 and those falling along the early A-type branch. The values for $[m_1]$ and $[u-b]$ and the value of $[c_1]$ are listed in Table 7. Due to

the large uncertainties in the relationship between photometric indices and spectral types we have gone no further than dividing the stars in three large groups:O-Type, B-type and A-type.

Those stars that in the V – c_1 diagram present a V magnitude much higher than expected for their spectral type are branded as non-members. Since the c_1 index is less affected by extinction than the $(b-y)$ color , this is a much more secure diagnostic than the V – $(b-y)$ diagram (see Figures 4 and 5). The star S3R1N13, which we have identified as a main-sequence B star from its position in the β – $[u-b]$ diagram, lies away from all other cluster members in both diagrams and is therefore branded as non-member. Several stars lying to the right of other cluster members in the V – $(b-y)$ diagram, grouped together with the members in the V – c_1 diagram. Since NGC 1893 is known to present differential reddening, we identify these stars as members with particularly high local reddening, something which is confirmed by the reddening estimation (see below).

Most stars whose parameters in the β – $[u-b]$ diagram identify as A-type stars present V magnitudes in the V – c_1 diagram much higher than expected for their spectral type and they turn out to be non-members. Only four stars lying close to the B9/A0 limit are considered likely members (S1R1N4, S2R2N25, S2R3N59 and S4R1N16). The list of all the stars that are identified as likely members is given in Table 8. For these stars we have calculated their color excess $E(b-y)$ using the iteration procedure given by Crawford (1978). These values are also listed in Table 8.

In the $E(b-y)$ – V diagram (see Figure 6) most cluster members concentrate in the $E(b-y) = 0.3-0.4$ range, but there are several stars displaying much higher reddenings. All these stars come from a relatively small spatial area within the cluster, which must be affected by local extinction. Leaving out this group of more highly reddened stars (including only stars with $E(b-y) < 0.4$), we determine an average cluster reddening of

$E(b-y) = 0.33 \pm 0.03$ from all the other members, where the uncertainty represents the standard deviation of the mean for the average. With this value we have calculated the intrinsic colors and magnitudes of all cluster members, which are listed in Table 8.

For all the stars classified as likely members, we have estimated a spectral type by using the temperature calibration from Napiwotzki et al. (1993). This calibration, based on the $[u-b]$ index, is valid for stars with $T_{\rm eff} \gtrsim 9500$ K and should therefore be valid for all members. By using the expression

$$\Theta \equiv \frac{5040 \text{ K}}{T_{\rm eff}} = 0.1692 + 0.2828[u-b] - [u-b]^2 \qquad (8)$$

we find the temperatures listed in Table 7. Once we have this information, we derive approximate spectral types by correlating the estimated $T_{\rm eff}$ with the average values for each spectral type from Kontizas & Theodossiou (1980). All objects are supposed to be unevolved and main-sequence values have been adopted. Of the eight B-type stars with spectroscopic classification, only three show agreement with the derived photometric temperature, all the others having photometric temperatures too low for their spectral type. However, this effect is not very large and in all cases implies differences of approximately 1 spectral subtype. Given the magnitude range covered by our observations, we must suspect that the temperature calibration is more accurate for later spectral types, because the photometric temperatures correspond well to the derived absolute magnitudes, even though there are no spectroscopic spectral types available for comparison.

3.3. H–R Diagram

Figures 7 and 8 show the $M_V - (b-y)_0$ and $M_V - c_0$ diagrams respectively. Fabregat & Torrejón (2000) have investigated the different photometric indices which are commonly used as horizontal axis in the observational HR diagrams, with regard to the B star region

of the main sequence and they conclude on the basis of four parameters (the span of values taken by the index over the B-star range, its intrinsic photometric accuracy, the ratio between the index variation and the accuracy and how the interstellar reddening affects the index) that the most efficient way to determine reliable ages for very young clusters is isochrone fitting to the observational $M_V - c_1$ HR diagram. As can be easily seen, the main sequence is far better defined in the $M_V - c_0$ diagram, confirming that c_0 is a much better spectral class indicator than $(b-y)_0$ for early type stars. We have plotted the empirical ZAMS from Balona & Shobbrook (1984) obtained from the relation $M_{VZAMS} = -2.769 + 9.599c_0 - 16.207c_0^2 + 17.716c_0^3 - 6.949c_0^4$ that represents analytically the adopted ZAMS in the $M_V - c_0$ diagram. Allowing for some uncertainty in the fit to the ZAMS, we find that the best value of the dereddened distance modulus is $V_0 - M_V = 13.9 \pm 0.2$. This value, although higher than those given by T91 and Fitzsimmons (1993), which are 13.2 and 13.4 respectively, is compatible within the errors with the latter, but is not compatible with the value given by T91. This discrepancy is due mainly to the value of reddening adopted by Fitzsimmons (1993) being nearer to our value than the value adopted by T91.

A second method of determining the distance to the cluster is by using the procedure from Balona & Shobbrook (1984) to estimate the absolute luminosities of all members from their β and c_0 indexes. We find that the values derived provide rather consistent values for the distance modulus. The average $V_0 - M_V$ is 13.2 ± 0.5, where the uncertainty is only due to the dispersion in the estimates and does not include the uncertainties in the determination of the individual M_V's.

By using this procedure, we find two stars (in addition to S3R1N4, which has been discussed above) which have absolute magnitudes which not only give values of $V_0 - M_V$ very far from the cluster average, but are inconsistent with their spectral types. These

are S4R3N2, which is about one magnitude too bright for the B2V spectral type given by Hiltner (1966) – which is perfectly consistent with the photometric indices – and S3R3N11, which is more than one magnitude too faint. Though it is unlikely finding a field B2V lying just in front of the cluster and at a similar distance, we brand S4R3N2 as a possible non-member. S3R3N11 has one of the highest reddenings measured, but it lies very close to cluster members with similar high reddening. Therefore its membership is also uncertain. Removing these two stars does not change significantly the estimate of $V_0 - M_V$.

The values of $V_0 - M_V$ obtained by fitting the ZAMS and by averaging the values derived from the individual estimation of M_V for members are rather different, but compatible within the errors (which are much larger for the second method). We prefer the first determination, not only because of its smaller intrinsic error, but also because the M_V's derived are more consistent with the spectral types. The four stars with higher effective temperature studied by Rolleston et al. (1993) all have $T_{\rm eff}$ in the range 25000 – 27500 K (and these values could be an underestimate according to Rolleston et al. 1993). Assuming $V_0 - M_V = 13.2$, these stars would all have absolute magnitudes > -3.4, while taking $V_0 - M_V = 13.9$, they have M_V's between -3.3 and -4.1, which correspond well with the derived spectral types between B0.2V and B0.7V (Vacca et al. 1996).

3.4. Emission-line candidates

We find several stars whose β indices indicate that they could have the Hβ line in emission. Their position in the M_V – c_0 diagram is compatible with their being Be stars (Marco et al. 2000). These objects, together with their dereddened indices, have been listed in Table 9.

We performed spectroscopy of all emission-line candidates (except for S5001, which

is too close to the brighter star S2R1N12 to allow separation unless seeing conditions are exceptional) and two other stars lying nearby in the $M_V - c_0$ diagram and having β indices close to the limiting $\beta < 2.55$, namely S4R2N14 and S2R1N16.

S4R2N15 was found to present no emission lines and a spectrum consistent with a K-type main sequence star and it is therefore not a cluster member. The spectrum of S4R2N14 shows no emission lines either, but strong Hα and Hβ absorption. It is most likely an F main-sequence star and therefore not a cluster member.

The three remaining stars (S1R2N23, S2R1N16 and S2R1N26) were all found to display Hα in emission. Their spectra (which are presented in Fig. 9 have low signal-to-noise ratios due to their faintness and do not cover the classification region. However, comparison with the stars in the digital atlas of Jacoby et al. (1984) indicates that they are all approximately F-type stars.

The earliest spectrum is that of S1R2N23, which is close to F0. This star also displays the strongest Hα among the group, with an Equivalent Width (EW) of -18Å. This line, as well as Hβ, probably displays inverse P-Cygni profiles, indicative of mass inflow, which are typically seen in many young stars. Also in emission is the Ca II $\lambda\lambda$ 8498, 8542, 8662 Å triplet. Measurements in previous studies (Hoag 1961; Cuffey 1973; Moffat & Vogt 1975; Massey et al. 1995) indicate strong variability, specially in the $(U - B)$ color.

The spectrum of S2R1N16 is that of a mid-F star and its Hα emission is rather weaker (EW$=-7$Å). The infrared Ca II triplet is in absorption and there is no evidence for other strong emission lines. Measurements in previous studies indicate very strong variability.

The latest spectrum is that of S2R1N26, which is very late F or early G. Its Hα emission is also the weakest, with an EW$=-5$Å. There is no evidence for any other emission lines. Previous photometric measurements are consistent with little variability.

The presence of emission lines identifies all three objects as young (pre-Main Sequence) stars. They are probably massive T Tauri stars, with S1R2N23 coming within the group of Herbig AeBe stars according to the classification of Thé et al. (1994), and they are all likely members of NGC 1893. Their intrinsic luminosities must be therefore much higher than those of main-sequence stars of the same spectral type.

3.5. Previously cataloged Be stars

We also observed the two NGC 1893 stars cataloged by Massey et al. (1995) as Be stars, namely S1R2N35 and S3R1N3. Their spectra are presented in Fig. 10. Both stars display very strong emission in Hα and Hβ, as well as in the upper Paschen lines (Pa14 to Pa17 are clearly seen in both stars). The O I λ7773 Å and λ8446 Å lines are also prominent. The yellow and red continuum is dominated by many strong permitted Fe II emission lines, among which the complex dominated by Fe II $\lambda\lambda$ 5169, 5198, 5235, 5276 Å is particularly strong in S3R1N3.

The strength of the Hα emission line (EW= -71Å) and the overall emission spectrum is compatible with an extreme classical Be star, but more typical of a Herbig Be young stellar object. The photometric indices of this star indicate that this object has a spectral type close to B0. Therefore, with $V = 13.6$, it is much fainter than expected (for example, it is 2.3 mag fainter than the B0.2V star S3R1N17). This could be indicating that it is surrounded by a local nebulosity and it is indeed a pre-main-sequence Herbig Be star. Classical Be stars tend on average to be brighter than corresponds to their spectral type (Fabregat & Torrejón 1998).

The emission spectrum of S1R2N35 is still stronger, with the EW of Hα amounting to -88 Å. Our blue spectrum of the source shows red-shifted emission components in Hγ and

Hδ. The spectral type is $\approx$ B0 and again the star is at least one magnitude too faint for the spectral type, indicating the presence of substantial local extinction. Therefore this star is most likely a Herbig Be object as well. References in the literature indicate that this star has brightened from $V \sim 12.8$ (Hoag 1961; Moffat & Vogt 1975) to $V \sim 12.3$ (Fitzsimmons 1993; Massey et al. 1995).

Schild & Romanishin (1976) list a third Be star in NGC 1983, which has been subsequently identified with S2R2N43 in the Webda database (Mermilliod 1999). However, we do not believe that this identification is correct. Massey et al. (1995) found no evidence of emission from S2R2N43. Rolleston et al. (1993) selected this star as a typical main-sequence early-B star from the photometric data of Fitzsimmons (1993) and studied its chemical composition using high-resolution spectroscopy without finding any indication of emission.

Our spectra of this star offer no evidence of emission in the whole optical range. We find a spectral type of B0.5V for S2R2N43, rather than the B1III derived by Massey et al. (1995). This spectral type is in agreement with the stellar parameters derived by Rolleston et al. (1993). Moreover, assuming that the reddening to the star is the average for the cluster, our measured $V = 11.5$ implies an absolute magnitude $M_V = -4.0$, which is that expected for the spectral type (Vacca et al. 1996). Therefore if there is another emission line B star in the cluster, it is not S2R2N43.

4. Discussion

We find a distance modulus $V_0 - M_V = 13.9 \pm 0.2$, moderately larger than that of previous authors. T91 give a rather lower $V_0 - M_V = 13.2 \pm 0.1$. There are two main contributions to this discrepancy. On the one hand, our derived $E(b-y) = 0.33 \pm 0.03$

implies an extinction $A_V = 1.42 \pm 0.13$, compared to the $A_V = 1.68 \pm 0.06$ from T91. Our determination of the reddening is based on a much larger sample of stars (but still leaving out all high-reddening members and all O-type stars). If the reddening of all member stars (including those with higher reddening, but leaving out O-type stars) is averaged, then a value $E(b-y) = 0.37 \pm 0.09$, much closer to that from T91 is obtained. However, because of the spatial concentration of the highly reddened members and the obvious gap between them and the rest of the cluster in the $E(b-y) - V$ diagram (see Figure 6), we are confident that the lower value $E(b-y) = 0.33 \pm 0.03$ is a more accurate measurement of the true interstellar reddening to the cluster.

In addition, most of the discrepancy in the distance modulus estimate comes from the fact that a higher value is needed in order to fit the ZAMS to the observational data. Our data include a much larger number of members than the work by T91 and Fitzsimmons (1993). Stars in the mid- and late-B range were very scarce in previous work, allowing for a looser fit of the ZAMS. As can be seen in Figure 8, the ZAMS from Balona & Shobbrook provides a very good lower envelope to stars from B1 to late B, but lies above the earliest B-type stars. It could be argued that the ZAMS should be fit to these B0-type stars, which would mean increasing the distance modules by an extra ~ 0.5 mag. However, this would mean that *all* the stars later than $\sim$ B1 have not yet reached the ZAMS, implying an age for the cluster of less than 1 Myr, which is in contradiction with the fact that at least some of the O-type stars seem to be close to the end of the main-sequence. The weak He II λ4686Å line in S3R2N15 has an EW very close to that considered the limit between main-sequence and giant stars (Mathys 1988), which would set the age of this star at ≈ 4 Myr for an assumed $M_* \geq 35 M_\odot$ at O5V (Vacca et al. 1996).

In any case, the presence of very massive Herbig Be stars indicates that star formation is still active in this cluster. Since stars in the mid-B range at least seem to have reached

the main sequence, this should be indicating that star formation has been going on for some time in NGC 1893. Further observations are needed in order to explore the possible existence of a larger pre-main-sequence population. The observed spectral distribution of pre-MS stars in NGC 1893 is indeed unexpected, suggesting that not all the pre-MS objects in the cluster have been observed. Moreover, since at least one O-type star seems to have an age ≈ 4 Myr, which is approximately the age assumed for the whole cluster by previous authors, good determinations of the ages of all the O stars are required in order to explore at which stage the most massive stars formed. Since massive stars are still forming, it may seem that massive stars can form both at the beginning or at end of the epoch of star formation. Knowing whether they can form at any given time will need in-depth study of the ages of all O-type stars in NGC 1893.

The identification of all emission-line objects as pre-MS stars means that there are no classical Be stars in NGC 1893. This is in agreement with the suggestion by Fabregat & Torrejón (2000) that there are no classical Be stars in clusters in which star formation is still active.

5. Conclusions

We have identified ≈ 50 very likely members of NGC 1893 and therefore we have a sample of likely members larger than previous studies (~ 24 members in T91 and ~ 30 members in Fitzsimmons 1993) to determine the cluster astrophysical parameters.

We derive a reddening to the cluster $E(b-y) = 0.33 \pm 0.03$. This value is similar to that obtained by Fitzsimmons (1993) but is incompatible with the value adopted by T91. We show that the reddening is variable across the face of the cluster and can reach much higher values than the average in some areas. If we include the highest values of individual

reddenings in the calculation of the average, then our value would be rather closer to the value given by T91. We have not adopted this value, because all the high values belong to stars coming from a relatively small spatial area within the cluster, which must be affected by local extinction.

We derive a distance modulus of 13.9 ± 0.2 by fitting the ZAMS from Balona & Shobbrook (1984). We obtain a higher value than the 13.2 obtained by T91 and the 13.4 by Fitzsimmons (1993), both based on a smaller number of likely members.

Five emission-line stars are shown to be pre-main-sequence objects, extending from about B0 to very late F spectral type. This suggests that several other pre-main-sequence objects could be present in this cluster, specially at fainter magnitudes than those observed by us. Further photometric and spectroscopic work must be conducted to confirm this suggestion.

The JKT and INT are operated on the island of La Palma by the Royal Greenwich Observatory in the Spanish Observatorio del Roque de Los Muchachos of the Instituto de Astrofísica de Canarias. The G.D. Cassini telescope is operated at the Loiano Observatory by the Osservatorio Astronomico di Bologna. We are thankful to all the staff at the Loiano Observatory for their support with the observations. This research has made use of data from the ING Archive. We would like to thank the Spanish CAT panel for allocating observing time to this project. AM would like to thank Dr. J. Fabregat for his help with the observations. IN acknowledges receipt of an ESA external research fellowship.

REFERENCES

Balona, L.A., and Shobbrook R.R. 1984, MNRAS, 211, 375

Canterna, R., Perry, C.L., and Crawford, D.L. 1979, PASP, 91, 263

Crawford, D.L., Mander, J. 1966, AJ, 71, 114

Crawford, D.L., Glaspey, J.W., and Perry, C.L. 1970a, AJ, 75, 822

Crawford, D.L., and Barnes, J.V. 1970b, AJ, 75, 978

Crawford, D.L., Barnes, J.V., and Hill, G. 1977, AJ, 82, 606

Crawford, D.L. 1978, AJ, 83, 48

Cuffey, J. 1973, AJ, 78, 747

Draper, P.W. 1998, Starlink User Note 139.7, R.A.L.

Fabregat, J., and Torrejón ,J.M. 1998, A&A, 332, 643

Fabregat, J., and Torrejón, J.M. 2000, A&A, 357, 451

Fitzsimmons, A., 1993, A&AS, 99, 15

Grønbech, B., Olsen, E.H., and Strömgren, B. 1976, A&AS, 26, 155

Hiltner, W.A. 1956, ApJS, 2, 389

Hiltner, W.A. 1966, IAU Symp.24, 373

Hoag, A.A., Johnson, H.L., Iriarte, B., Mitchell, R.J., Hallam, K.L., and Sharpless, S. 1961, Publ. U.S. Naval Obs. Sec. Ser. XVII, part VII

Hoag, A.A., and Applequist, L. 1965, ApJS, 12, 215

Howarth, I., Murray, J., Mills, D., and Berry, D.S. 1997, Starlink User Note 50.20, R.A.L.

Jacoby, G.H., Hunter, D.A., and Christian, C.A. 1984, ApJS, 56, 257

Johnson, H.L., and Morgan, W.W. 1955, ApJ, 122, 429

Kontizas, E., and Theodossiou, E. 1980, MNRAS, 192, 745

Manfroid, J. 1993, A&A, 271, 714

Manfroid, J., and Sterken, C. 1987, A&A, 71, 539

Marco, A., Bernabeu, G., Fabregat, J., and et al. 2000, In: Smith M., Henrichs H.F., Fabregat J. (eds.) IAU Colloq. 175, The Be Phenomenon in Early-Type Stars. ASP Conference Series, 2000, Vol. 214, 59, San Francisco

Moffat, A.F.J., and Vogt, N. 1975, A&AS, 20, 85

Massey, P., Johnson, K.E., and DeGioia-Eastwood, K. 1995, ApJ, 454, 151

Mathys, G. 1988, A&AS, 76, 427

Mermilliod, J.C. 1998, WEBDA data base, http://obswww.unige.ch/webda/information.html

Moffat, A.F.J., and Vogt, N. 1975, A&AS, 20, 85

Napiwotzki, R., Schönberner, and Wenske V. 1993, A&A, 268, 653

Perry, C.L., Lee, P.D., and Barnes, J.V. 1978, PASP, 90, 73

Perry, C.L., Olsen, E.H., and Crawford, D.L. 1987, PASP, 99, 1184

Rolleston, W.R.J., Brown, P.J.F., Dufton, P.L., and Fitzsimmons A. 1993, A&A, 270, 107

Schild, R.E, and Romanishin, W. 1976, ApJ, 204, 493

Shobbrook, R.R. 1983, MNRAS, 205, 1215

Shortridge, K., Meyerdicks, H., Currie, M., and et al. 1997, Starlink User Note 86.15, R.A.L

Steele, I.A., Negueruela, I., and Clark, J.S. 1999, A&AS, 137, 147

Stetson, P.B. 1987, PASP, 99, 191

Strömgren, B. 1966, ARA&A, 4, 433

Tapia, M., Costero, R., Echevarría, J., and Roth, M. 1991, MNRAS, 253, 649 (T91)

Thé, P.S., de Winter, D., and Pérez, M.R. 1993, A&AS, 104, 315

Vacca, W.D., Garmany, C.D., and Shull, J.M. 1996, ApJ, 460, 914

Vallenari, A., Richichi, A., Carraro, G., and Girardi L. 1999, A&A, 349, 825

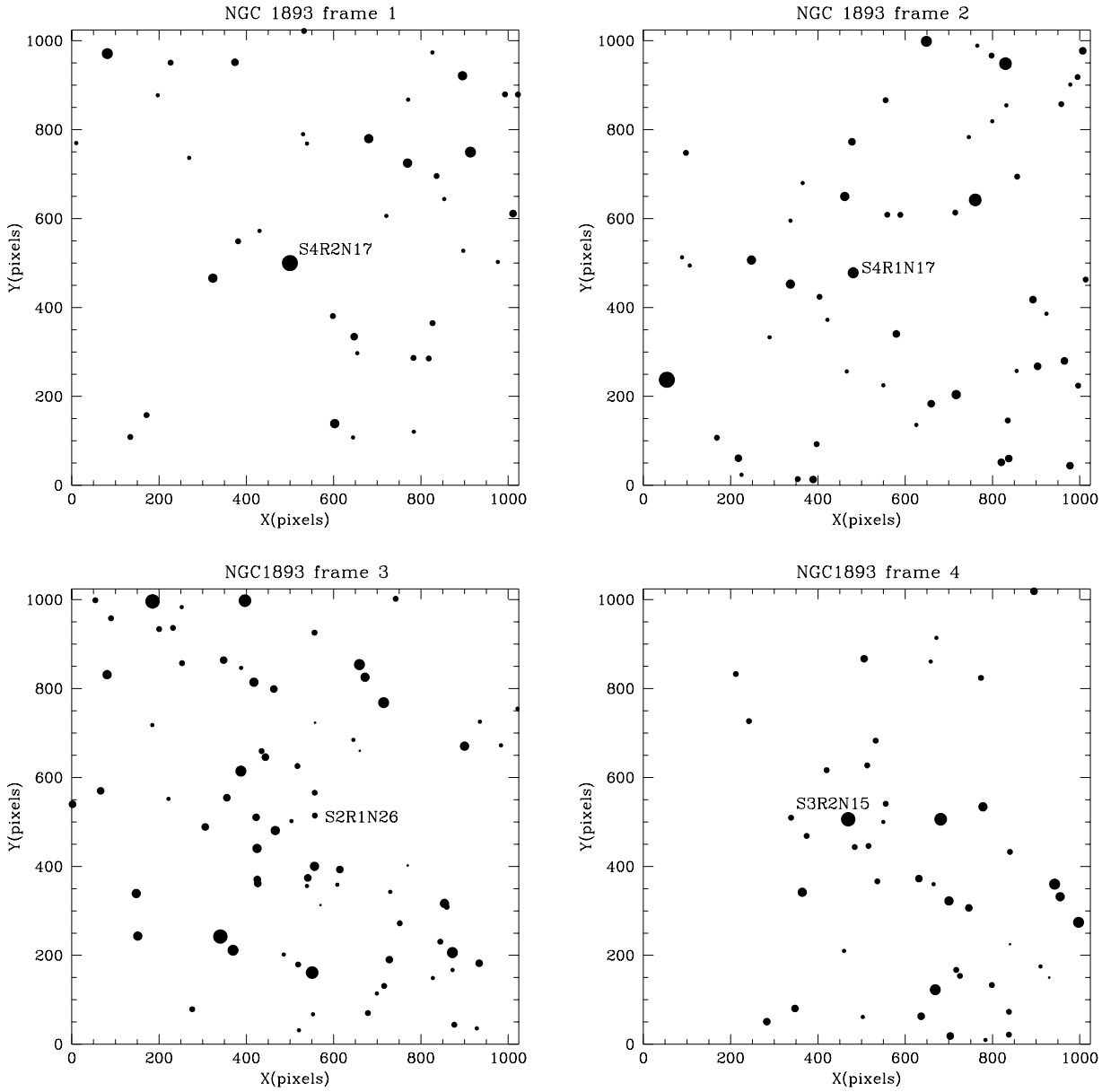

Fig. 1.— (a)-(d). Schematic maps of the four region observed in NGC 1893. The size of the dots represents relative brightness of stars in the field. North is down and East left in all fields.

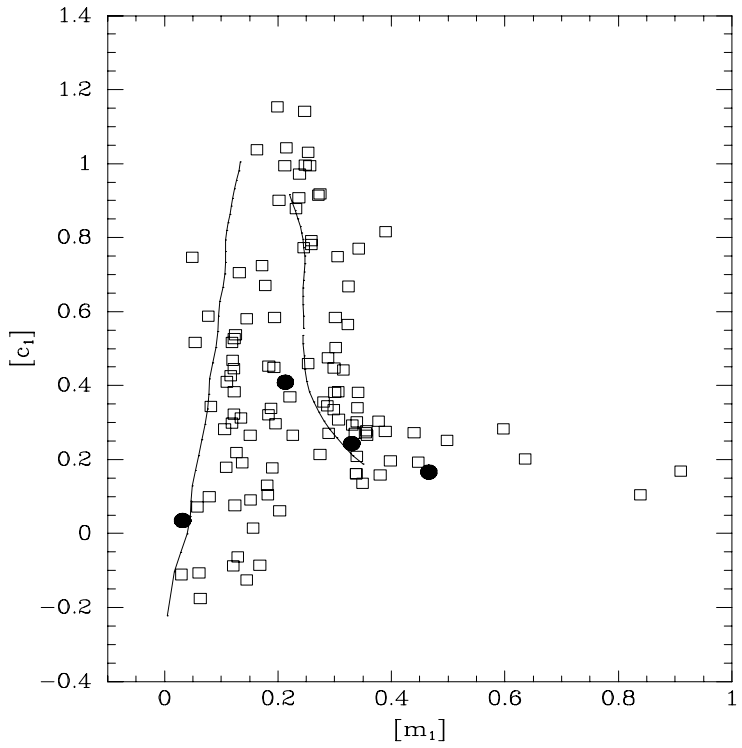

Fig. 2.— The $[c_1] - [m_1]$ diagram for all the stars observed in the field of NGC 1893. The thin solid lines represent the average loci of field B-type (left) and A-type (right) main sequence stars. Filled circles represent stars with Hβ in emission.

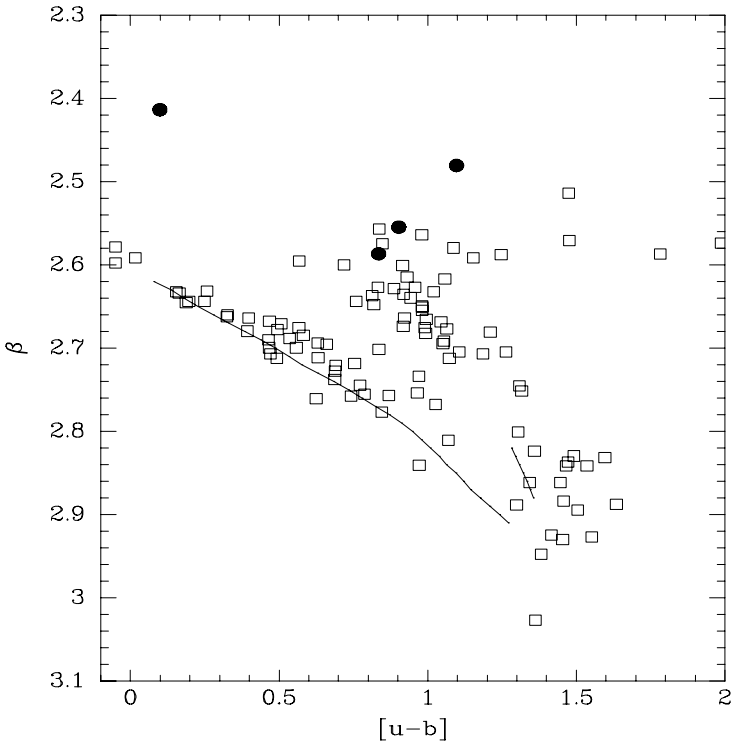

Fig. 3.— The $\beta - [u-b]$ diagram for all the stars observed in the field of NGC 1893. The thin lines represent the loci of main-sequence B stars (long line) and main-sequence A1–A2 stars (short line). The turnover in the $\beta - [u-b]$ correlation occurs approximately at spectral type A0. Filled circles represent stars with Hβ in emission.

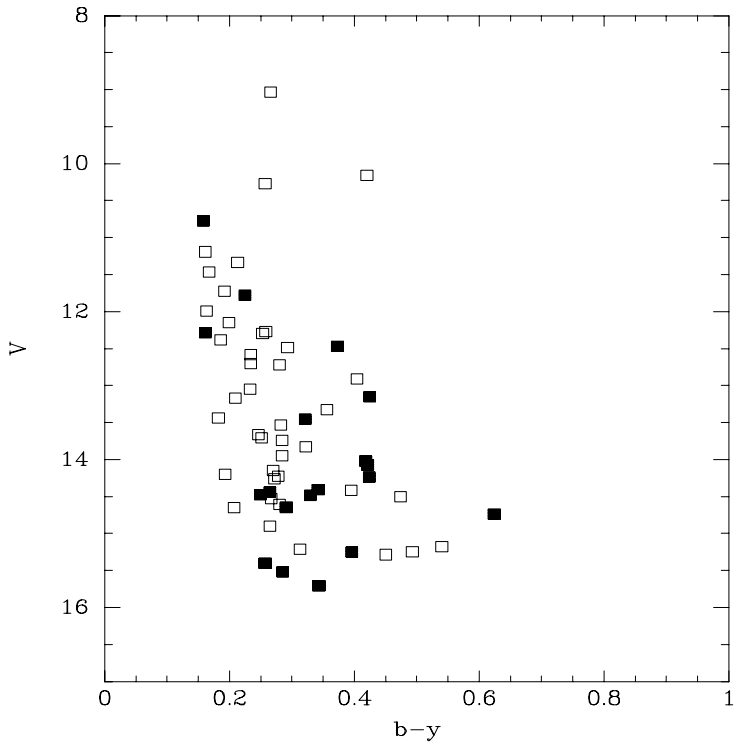

Fig. 4.— V magnitude against $(b-y)$ color for suspected members of NGC 1893. Filled squares represent stars that have finally been classed as non-members, while open squares represent those that have been considered very likely members.

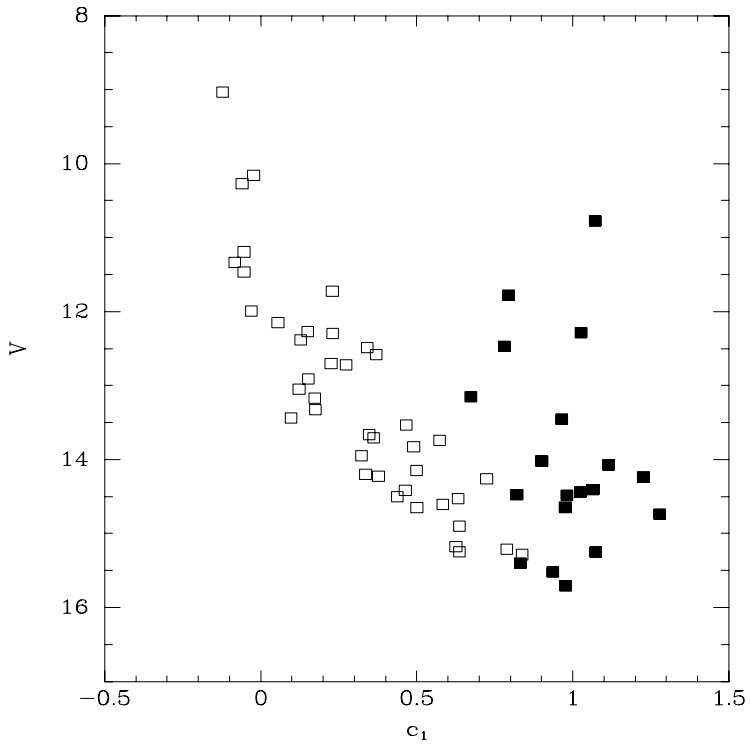

Fig. 5.— V magnitude against c_1 index for suspected members of NGC 1893. Filled squares represent stars that have finally been classed as non-members, while open squares represent those that have been considered very likely members.

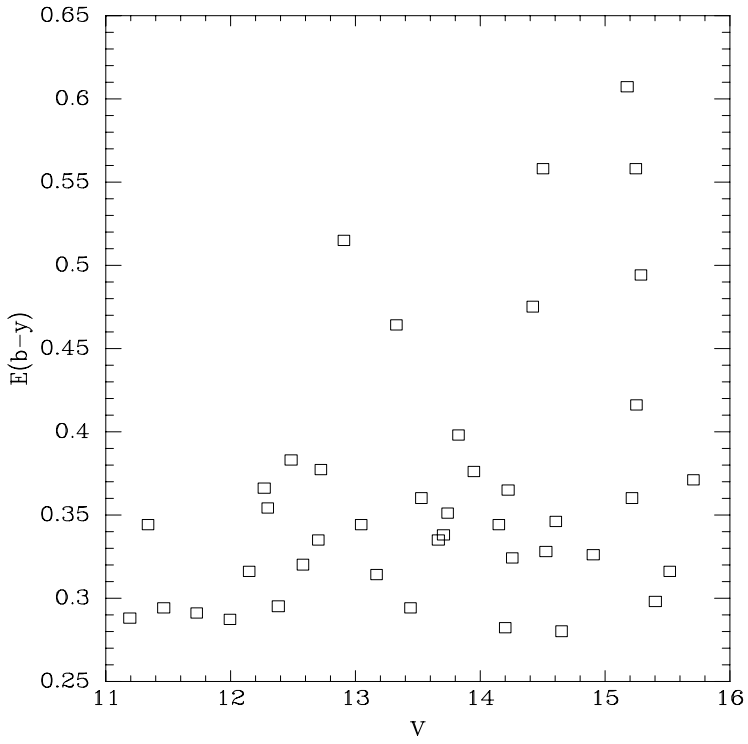

Fig. 6.— Individual color excess $E(b-y)$, calculated by applying Crawford's (1978) procedure, against apparent visual magnitude for all likely members of NGC 1893.

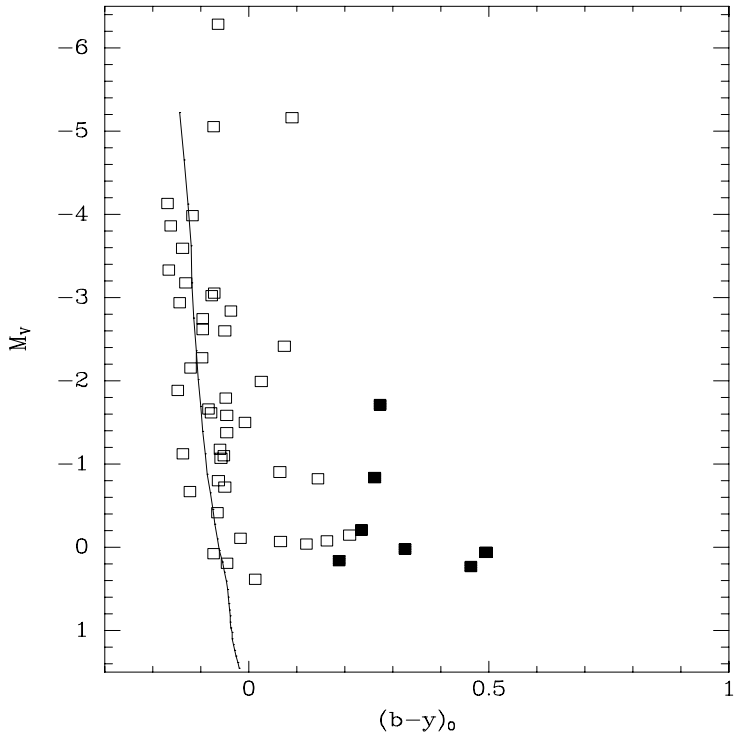

Fig. 7.— Absolute magnitude M_V (calculated using the average distance modulus for the cluster) against $(b-y)_0$ color. Filled squares represent stars studied spectroscopically. The solid line represents the theoretical ZAMS from Perry et al. (1987).

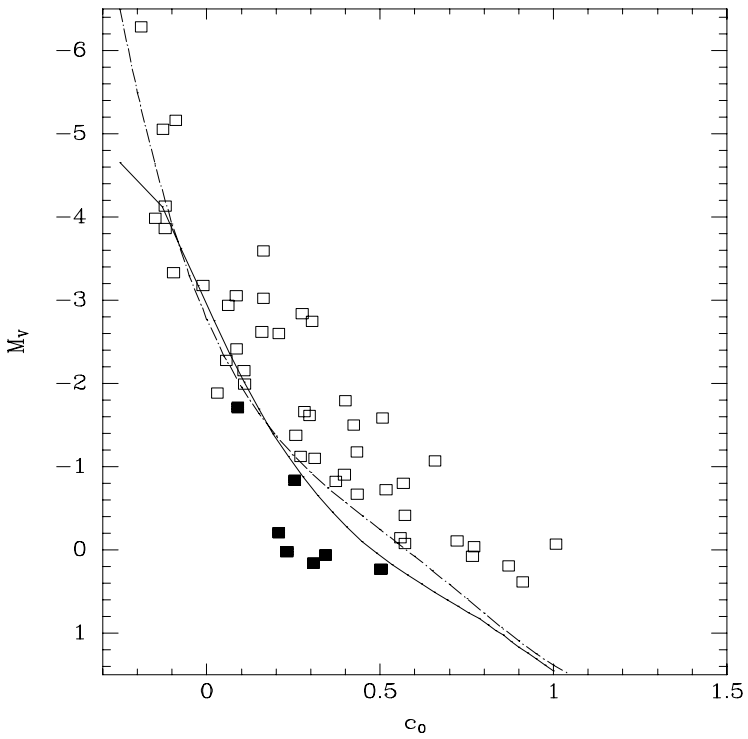

Fig. 8.— Absolute magnitude M_V (calculated using the average distance modulus for the cluster) against c_0 index. Filled squares represent stars studied spectroscopically. The solid line represents the theoretical ZAMS from Perry et al. (1987). The dashed line represents the theoretical ZAMS from Balona & Shobbrook (1984).

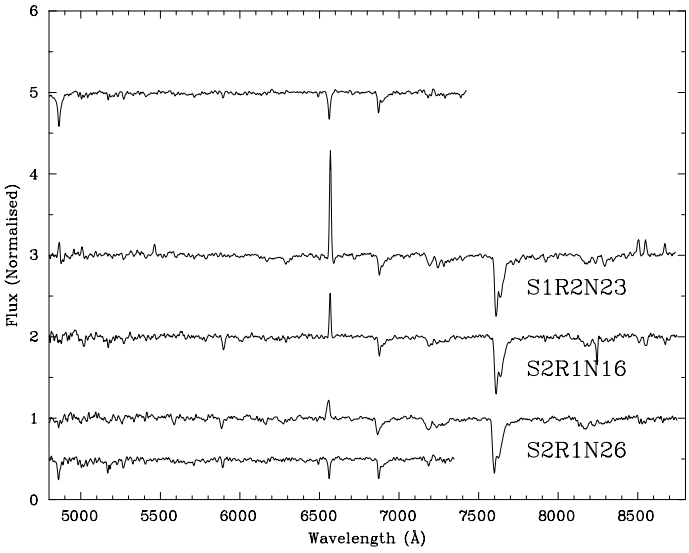

Fig. 9.— Low resolution spectra of the three candidate emission-line stars which were actually found to display Hα in emission. Also shown for comparison are the spectra of HD 10032 (F0V, top) and HD 31084 (F9V, bottom) from the electronic atlas of Jacoby et al. (1984), binned to the same resolution. All the spectra have been divided by a spline fit to the continuum for normalisation and arbitrarily offset for display.

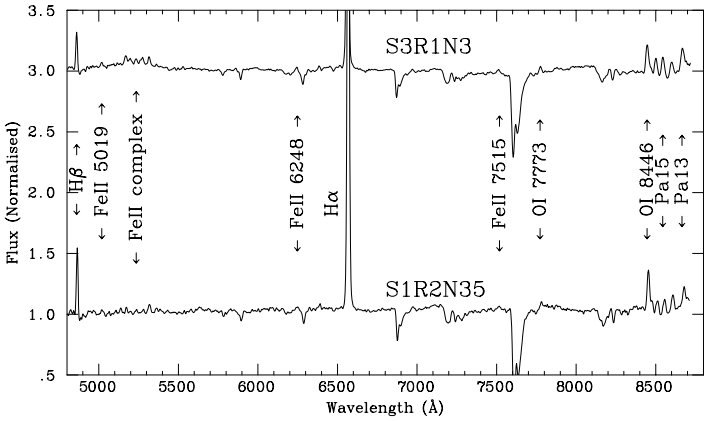

Fig. 10.— Low resolution spectra of the two stars in NGC 1893 previously cataloged as Be stars, S1R2N35 and S3R1N3. The spectra have been divided by a spline fit to the continuum for normalisation.

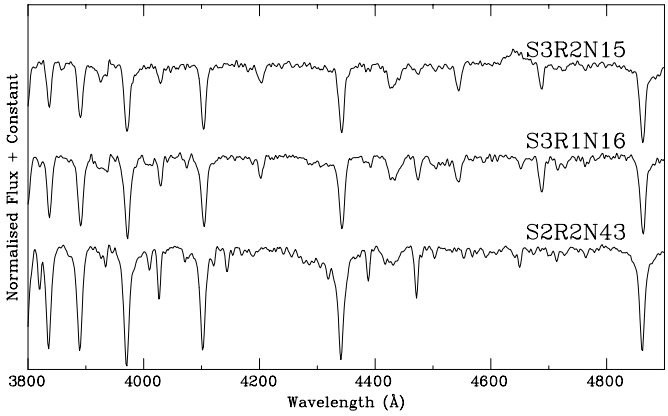

Fig. 11.— Spectra of bright stars in NGC 1893 for which our spectral classification differs from previous estimates. In S3R2N1 (top), the very weak He I λ4471Å, together with He I+ He II λ4026Å $\simeq$ He II λ4200Å, makes the star earlier than O6V. The quantitative criterion of Mathys (1988) places the star on the limit between O5V and O5.5V. The weakness of He II λ4686Å and strength of N III emission point to the star's being slightly evolved from the main sequence. In S3R1N16 (middle), the condition He I λ4471Å $\simeq$ He II λ4541Å defines O7V. In S2R2N43, the weak Si lines mark the star as main sequence, while the strength of the O II spectrum indicates B0.5V.

Table 1. Observational details of the photometry. Observations were taken using the 1.0-m JKT on December 11th and December 22nd 1997 for four frames.

	Central Star	Coordinates (1950)
#1	S4R2N17	α=5h 19m 12.00s δ=+33° 28′ 00″.4
#2	S4R1N17	α=5h 19m 23.24s δ=+33° 26′ 40″.0
#3	S2R1N26	α=5h 19m 31.09s δ=+33° 22′ 11″.3
#4	S3R2N15	α=5h 19m 22.63s δ=+33° 19′ 29″.0

Table 2. Standard stars with their cataloged values and spectral types taken from literature.

Number	V	$(b-y)$	m_1	c_1	β	Spectral Type
			h Persei			
837	14.080	0.393	0.000	0.918	2.801	
843	9.320	0.277	-0.050	0.166		B1.5V
867	10.510	0.393	0.161	0.375	2.613	
869					2.700	
935	14.020	0.362	-0.004	0.854	2.802	
950	11.290	0.318	-0.048	0.214	2.642	B2V
960					2.767	
978	10.590	0.305	-0.039	0.177	2.643	B2V - B1.5V
982					2.796	
1015	10.570	0.225	0.033	0.741		B8V
1078	9.750	0.316	-0.065	0.167	2.610	B1V - B1Vn
1181	12.650	0.372	-0.034	0.379	2.718	
			χ Persei			
2133					2.676	
2139	11.380	0.255	-0.033	0.196	2.649	B2V

Table 2—Continued

Number	V	$(b-y)$	m_1	c_1	β	Spectral Type
2147	14.340	0.406	-0.050	1.002	2.863	
2167	13.360	0.352	-0.056	0.627	2.752	
2185	10.920	0.283	-0.049	0.406	2.700	B2Vn
2196	11.570	0.250	-0.006	0.210	2.670	B1.5V
2200					2.721	
2232	11.110	0.292	-0.105	0.207	2.651	B2V
2235	9.360	0.316	-0.088	0.150	2.611	B1V
2251	11.560	0.302	-0.042	0.349	2.709	B3V
			NGC 2169			
11	10.600	0.084	0.065	0.541	2.698	B8V
15	11.080	0.130	0.109	0.944	2.864	B9.5V
18	11.800	0.115	0.105	0.912	2.872	B9.5V
			NGC 6910			
7	10.360	0.670	-0.160	0.110	2.612	B0.5V
11	10.900	0.770	0.420	0.430	2.555	
13	11.720	0.660	-0.140	0.220	2.647	B1V

Table 2—Continued

Number	V	$(b-y)$	m_1	c_1	β	Spectral Type
14	11.730	0.590	-0.100	0.220	2.652	B1V
15	12.220	0.590	-0.110	0.330	2.679	
17	12.660	0.670	-0.120	0.310	2.659	
18	12.810	0.750	-0.140	0.290	2.680	
19	12.920	0.640	-0.120	0.380	2.662	
20	12.980	0.610	-0.130	0.420	2.692	
			NGC 1039			
92	11.960	0.303	0.138	0.481	2.678	
96	9.740	0.086	0.176	0.973	2.890	
97	11.820	0.144	0.198	0.900	2.855	
102	10.760	0.151	0.194	0.894	2.848	
105	11.220	0.176	0.204	0.796	2.817	
109	10.030	0.066	0.152	1.013	2.916	
111	9.950	0.055	0.163	1.021	2.908	

Table 3. Catalog of 41 standard stars observed and transformed to the Crawford-Barnes *uvby* and the Crawford-Mander $H\beta$ standard systems. The internal rms errors of the mean measure in the transformation of each star are given in columns 8 to 11 in units of 0.001 mag. Columns 12 to 16 give the difference Δ=standard value minus transformed value, in units of 0.001 mag. N is the number of measures of each standard star in the transformation in V, $(b-y)$, m_1, c_1. The number of measures in β is one for each standard star in the transformation.

Star	V	$(b-y)$	m_1	c_1	β	N_{uvby}	σ_V	$\sigma_{(b-y)}$	σ_{m_1}	σ_{c_1}	Δ_V	$\Delta_{(b-y)}$	Δ_{m_1}	Δ_{c_1}	Δ_β
h Persei															
869	-	-	-	-	2.724	-	-	-	-	-	-	-	-	-	-024
837	14.095	0.411	-0.031	0.907	2.789	3	006	009	024	024	-016	-019	032	011	012
843	9.330	0.319	-0.151	0.240	-	1	-	-	-	-	-010	-042	101	-074	-
867	10.572	0.376	0.177	0.379	2.666	5	006	008	013	025	-063	016	-015	-005	-053
935	14.051	0.411	-0.076	0.856	2.781	6	018	007	018	038	-031	-049	073	-003	021
950	11.297	0.337	-0.079	0.221	2.630	1	-	-	-	-	-007	-019	031	-007	012
960	-	-	-	-	2.727	-	-	-	-	-	-	-	-	-	040
978	10.646	0.328	-0.070	0.194	2.634	5	016	013	016	023	-056	-023	031	-017	009
982	-	-	-	-	2.779	-	-	-	-	-	-	-	-	-	017
1015	10.573	0.223	0.029	0.677	-	2	037	023	006	030	-003	003	005	064	-
1078	9.775	0.317	-0.043	0.138	2.611	3	008	021	042	036	-025	-002	-021	030	-001
1181	12.655	0.352	-0.008	0.338	2.703	6	022	022	044	030	-006	020	-025	041	015
χ Persei															
2133	-	-	-	-	2.658	-	-	-	-	-	-	-	-	-	018
2139	11.351	0.298	-0.097	0.235	2.641	2	011	024	030	007	029	-043	064	-039	008
2147	14.359	0.392	-0.083	1.022	2.783	5	023	034	051	051	-019	013	033	-020	080
2167	13.364	0.347	-0.080	0.616	2.733	6	012	008	012	024	-004	005	025	011	019
2185	10.926	0.275	-0.018	0.412	2.688	3	008	013	038	044	-006	008	-031	-006	012
2196	11.549	0.304	-0.066	0.246	2.632	6	012	013	023	023	021	-052	056	-034	038
2200	-	-	-	-	2.707	-	-	-	-	-	-	-	-	-	014
2232	11.052	0.238	-0.029	0.177	2.639	4	013	013	041	035	058	054	-077	030	012
2235	9.365	0.311	-0.071	0.131	2.575	3	012	015	046	039	-005	005	-016	018	036
2251	11.563	0.297	-0.028	0.367	2.689	6	009	011	027	030	-004	004	-013	-018	020
NGC 2169															
11	10.538	0.076	0.061	0.545	2.719	1	-	-	-	-	062	008	004	-004	-021

Table 3—Continued

Star	V	$(b-y)$	m_1	c_1	β	N_{uvby}	σ_V	$\sigma_{(b-y)}$	σ_{m_1}	σ_{c_1}	Δ_V	$\Delta_{(b-y)}$	Δ_{m_1}	Δ_{c_1}	Δ_β
15	11.023	0.122	0.092	0.939	2.856	1	-	-	-	-	057	008	017	005	008
18	11.733	0.053	0.260	0.813	2.883	1	-	-	-	-	067	062	-155	099	-011
NGC 6910															
7	10.320	0.667	-0.150	0.092	2.652	2	011	004	012	016	041	003	-011	018	-040
11	-	-	-	-	2.639	-	-	-	-	-	-	-	-	-	-084
13	11.681	0.619	-0.082	0.211	2.661	2	004	023	038	004	039	041	-058	009	-014
14	11.730	0.569	-0.053	0.201	2.678	2	004	028	040	018	001	021	-048	019	-026
15	12.193	0.609	-0.134	0.359	2.698	2	007	006	014	002	027	-019	024	-029	-019
17	12.635	0.700	-0.149	0.294	2.688	2	008	010	025	040	025	-030	029	017	-029
18	12.816	0.755	-0.132	0.296	2.705	2	014	004	006	048	-006	-005	-009	-006	-025
19	12.897	0.610	-0.065	0.402	2.709	2	025	035	037	047	023	031	-056	-022	-047
20	12.920	0.619	-0.118	0.446	2.730	2	016	001	019	006	060	-009	-013	-026	-038
NGC 1039															
92	11.928	0.282	0.150	0.520	2.709	1	-	-	-	-	032	021	-012	-039	-031
96	9.703	0.063	0.219	0.976	2.887	1	-	-	-	-	037	023	-043	-003	003
97	11.782	0.129	0.215	0.934	2.838	1	-	-	-	-	038	015	-017	-034	017
102	10.724	0.150	0.193	0.893	2.851	1	-	-	-	-	036	001	001	001	-003
105	11.166	0.167	0.232	0.971	2.832	1	-	-	-	-	054	009	028	-175	-015
109	10.034	0.040	0.178	1.018	2.960	1	-	-	-	-	-004	026	-026	-005	-044
111	9.900	0.025	0.249	0.964	2.927	1	-	-	-	-	050	030	-086	057	-019

Table 4. Mean catalog minus transformed values for the standard stars and their standard deviations in V, (b−y), m_1, c_1 and β.

Δ_m(V)	Δ_m(b−y)	$\Delta_m(m_1)$	$\Delta_m(c_1)$	$\Delta_m(\beta)$
0.014	0.003	−0.005	−0.004	−0.003
0.033	0.027	0.049	0.044	0.031

Table 5. Observational details of the optical spectroscopy. Observations were taken using the 1.52-m G. D. Cassini telescope and BFOSC. All dates refer to February 2000.

Star	Observation Date(s)	Resolution
S1R2N23	3/2	220 Å/mm
S1R2N35	3/2	220 Å/mm, 170 Å/mm
S2R1N16	3/2	220 Å/mm
S2R1N18	4/2	170 Å/mm
S2R1N26	3/2, 6/2	220 Å/mm
S2R2N43	3/2, 4/2	220 Å/mm, 120 Å/mm
S3R1N3	3/2	220 Å/mm
S3R1N16	4/2	170 Å/mm
S3R1N17	4/2	170 Å/mm
S3R2N15	4/2	170 Å/mm
S4R2N14	3/2	220 Å/mm
S4R2N15	3/2	220 Å/mm

Table 6. Pixel coordinates and measured photometric parameters for all the stars in the field of NGC 1893.

Star	Frame	X Position	Y Position	V	b−y	m_1	c_1	β	N_{uvby}	N_β
S1R1N2	#2	745.8	783.4	-	-	-	-	2.511	-	1
S1R1N4	#2	799.5	818.9	15.707	0.343	0.127	0.977	2.948	2	2
S1R1N5	#2	831.8	854.8	-	-	-	-	2.560	-	1
S1R1N7	#3	678.5	70.1	14.653	0.207	0.187	0.500	2.754	2	2
S1R1N8	#3	699.0	114.2	-	-	-	-	2.891	-	1
S1R1N9	#3	715.8	131.2	14.946	0.540	0.207	0.267	2.636	2	2
S1R1N10	#3	876.5	43.9	14.604	0.280	0.033	0.583	2.745	1	1
S1R1N18	#2	856.6	694.4	14.469	0.366	0.223	0.413	2.633	1	1
S1R1N19	#2	760.6	642.0	11.100	0.724	0.607	0.249	2.587	1	1
S1R2N1	#2	820.3	51.7	14.224	0.278	0.094	0.377	2.738	1	1
S1R2N2	#2	837.3	60.2	13.744	0.300	0.228	0.728	2.752	1	1
S1R2N4	#2	977.5	44.2	14.074	0.421	0.118	1.115	2.842	1	1
S1R2N6	#2	835.0	145.8	15.214	0.313	0.072	0.788	2.811	1	1
S1R2N19	#2	903.4	267.7	14.020	0.418	0.256	0.900	2.832	1	1
S1R2N20	#2	964.6	279.9	13.330	0.356	0.068	0.175	2.668	1	1
S1R2N21	#2	996.3	224.2	-	-	-	-	2.621	-	1
S1R2N22	#2	892.7	417.7	14.183	0.361	0.183	0.520	2.669	1	1
S1R2N23	#2	923.6	386.0	15.344	0.655	0.256	0.297	2.481	1	1
S1R2N25	#2	1013.	462.9	15.031	0.398	0.262	0.356	2.692	1	1
S2R1N1	#3	933.5	182.2	14.257	0.272	0.091	0.724	2.768	1	1
S2R1N2	#3	872.2	206.2	12.148	0.199	0.092	0.055	2.660	1	1
S2R1N3	#3	844.4	230.7	14.526	0.267	0.060	0.633	2.757	1	1

Table 6—Continued

Star	Frame	X Position	Y Position	V	b−y	m_1	c_1	β	N_{uvby}	N_β
S2R1N4	#3	872.5	167.0	15.737	0.589	0.127	0.560	2.713	1	1
S2R1N7	#3	727.8	190.3	13.441	0.182	0.145	0.097	2.700	2	2
S2R1N9	#3	751.5	272.1	14.404	0.342	0.139	1.064	2.830	1	1
S2R1N11	#3	729.6	342.7	15.868	0.467	0.174	0.658	2.681	1	1
S2R1N12	#3	854.0	316.7	12.704	0.234	0.115	0.225	2.700	1	1
S2R1N15	#3	614.3	393.1	14.199	0.193	0.134	0.336	2.728	1	1
S2R1N16	#3	608.4	358.8	15.556	0.793	-0.041	0.568	2.587	1	1
S2R1N18	#3	550.8	161.2	11.193	0.161	0.116	-0.054	2.644	2	2
S2R1N19	#3	518.7	179.4	15.007	0.572	0.119	0.616	2.705	2	2
S2R1N23	#3	540.8	374.2	13.705	0.251	0.055	0.362	2.685	1	1
S2R1N24	#3	556.2	400.3	12.722	0.280	0.037	0.274	2.707	1	1
S2R1N25	#3	466.4	480.8	13.048	0.233	0.049	0.123	2.663	1	1
S2R1N26	#3	503.4	502.0	15.386	0.824	0.066	0.408	2.555	1	1
S2R1N27	#3	557.0	514.4	15.059	0.589	0.252	0.391	2.592	2	2
S2R1N28	#3	556.6	565.8	15.083	0.477	0.121	0.308	2.644	2	2
S2R1N31	#3	517.1	626.0	14.439	0.265	0.153	1.024	2.862	2	2
S2R2N20	#3	900.0	670.5	13.171	0.209	0.114	0.173	2.713	1	1
S2R2N25	#3	935.2	725.7	15.403	0.257	0.177	0.832	2.889	1	1
S2R2N35	#3	742.2	1002.1	14.860	0.383	0.275	0.274	2.683	1	1
S2R2N40	#4	745.9	306.7	13.826	0.322	0.014	0.490	2.696	3	3
S2R2N41	#3	714.7	768.4	11.995	0.163	0.077	-0.030	2.656	3	3
S2R2N42	#3	672.0	825.7	12.383	0.186	0.092	0.128	2.680	3	3

Table 6—Continued

Star	Frame	X Position	Y Position	V	b−y	m_1	c_1	β	N_{uvby}	N_β
S2R2N43	#3	659.1	854.0	11.465	0.167	0.068	-0.054	2.633	3	3
S2R2N45	#4	840.0	432.7	14.483	0.329	0.166	0.981	2.884	2	2
S2R2N46	#4	778.1	534.2	12.514	0.525	0.112	0.461	2.601	2	2
S2R3N59	#4	773.6	824.1	15.251	0.396	0.085	1.073	2.925	1	1
S3R1N1	#3	387.5	614.5	12.269	0.258	-0.004	0.151	2.632	3	3
S3R1N2	#3	355.5	554.5	13.664	0.246	0.040	0.348	2.689	3	3
S3R1N3	#3	305.8	488.8	13.612	0.603	-0.161	0.156	2.414	1	1
S3R1N4	#3	422.6	510.5	13.948	0.284	0.060	0.323	2.596	3	3
S3R1N6	#3	424.5	440.5	12.485	0.293	0.012	0.341	2.678	1	1
S3R1N8	#3	425.1	370.7	13.738	0.284	0.028	0.573	2.719	1	1
S3R1N9	#3	221.7	552.0	-	-	-	-	2.644	-	1
S3R1N12	#3	147.8	339.0	12.472	0.373	0.013	0.780	2.734	1	1
S3R1N13	#3	151.3	243.4	13.151	0.425	-0.059	0.673	2.758	1	1
S3R1N16	#3	340.5	242.3	10.273	0.257	-0.052	-0.060	2.598	1	1
S3R1N17	#3	369.5	211.5	11.339	0.213	0.077	-0.083	2.634	2	2
S3R2N1	#4	681.2	506.1	10.774	0.148	0.168	1.072	2.837	3	3
S3R2N2	#4	700.4	322.4	12.579	0.234	0.047	0.370	2.676	3	3
S3R2N4	#4	631.4	372.6	13.530	0.282	0.020	0.466	2.694	3	3
S3R2N5	#4	536.2	366.4	14.420	0.395	-0.003	0.463	2.712	2	2
S3R2N6	#3	435.0	659.4	14.756	0.604	0.052	0.894	2.705	2	2
S3R2N7	#3	443.7	646.0	14.336	0.428	0.026	1.123	3.027	2	2
S3R2N8	#4	484.3	443.6	15.049	0.490	-0.037	0.566	3.348	2	2

Table 6—Continued

Star	Frame	X Position	Y Position	V	b−y	m_1	c_1	β	N_{uvby}	N_β
S3R2N9	#4	516.0	446.0	15.245	0.493	-0.033	0.637	2.756	2	2
S3R2N13	#4	420.1	616.5	15.286	0.450	-0.095	0.837	2.777	1	1
S3R2N15	#4	469.5	506.1	10.161	0.420	-0.073	-0.023	2.592	3	3
S3R2N16	#4	338.5	509.6	14.738	0.624	-0.001	1.279	2.927	2	2
S3R2N17	#4	374.1	468.6	15.063	0.481	0.153	0.404	2.664	2	2
S3R2N18	#4	364.2	341.9	12.907	0.404	-0.071	0.152	2.646	3	3
S3R2N26	#3	66.2	570.1	13.456	0.321	0.099	0.965	2.801	3	3
S3R2N27	#4	282.9	50.8	14.204	0.371	0.065	0.526	2.648	1	1
S3R3N7	#4	505.9	867.2	13.293	0.419	0.154	0.559	2.695	2	2
S3R3N11	#4	532.4	682.9	14.502	0.474	-0.070	0.438	2.671	1	1
S3R3N12	#4	242.0	726.8	14.383	0.551	0.050	0.376	2.600	1	1
S3R3N13	#4	211.8	832.9	15.177	0.540	-0.119	0.625	2.761	1	1
S4R1N1	#2	555.1	866.2	14.712	0.519	0.173	0.312	2.629	2	2
S4R1N4	#2	478.1	772.8	13.956	0.345	0.231	0.450	2.677	1	1
S4R1N8	#2	461.5	649.8	13.184	0.386	0.163	0.422	2.674	3	3
S4R1N10	#2	559.0	608.7	14.905	0.265	0.109	0.637	2.841	2	2
S4R1N11	#2	588.8	608.5	14.793	0.398	0.230	0.346	2.650	1	1
S4R1N13	#2	714.7	613.4	14.388	0.420	0.243	0.387	2.617	1	1
S4R1N16	#2	337.2	595.2	15.519	0.285	0.141	0.936	2.862	2	2
S4R1N17	#2	480.9	478.2	11.780	0.225	0.233	0.794	2.824	3	3
S4R2N3	#1	226.5	950.8	14.475	0.249	0.262	0.820	2.930	1	1
S4R2N7	#1	373.9	951.7	14.239	0.424	0.111	1.226	2.888	1	1

Table 6—Continued

Star	Frame	X Position	Y Position	V	b−y	m_1	c_1	β	N_{uvby}	N_β
S4R2N9	#2	97.7	747.9	14.985	0.488	0.200	0.375	2.676	2	2
S4R2N12	#2	106.4	494.5	15.333	0.504	0.032	0.550	2.702	2	2
S4R2N14	#1	430.3	572.3	15.482	0.518	0.123	0.374	2.575	1	1
S4R2N15	#1	381.2	549.0	14.488	0.592	0.447	0.320	2.514	1	1
S4R2N17	#1	500.0	500.0	9.036	0.266	-0.022	-0.123	2.579	1	1
S4R2N18	#2	247.7	506.7	12.297	0.253	0.028	0.230	2.664	3	3
S4R2N19	#2	337.0	452.5	12.284	0.161	0.204	1.026	2.895	3	3
S4R2N20	#2	403.7	424.0	14.606	0.448	0.188	0.384	2.627	2	2
S4R2N22	#2	579.6	340.6	13.856	0.342	0.192	0.652	2.707	3	3
S4R2N23	#2	289.3	333.1	15.613	0.488	0.065	0.468	2.637	2	2
S4R2N24	#2	466.2	256.1	15.820	0.424	0.213	0.220	2.627	1	1
S4R2N27	#2	659.7	183.4	13.702	0.401	0.208	0.351	2.640	1	1
S4R2N28	#2	716.8	204.1	13.286	1.022	0.583	0.372	2.574	1	1
S4R2N29	#1	598.3	380.9	14.490	0.591	0.408	0.401	2.571	2	2
S4R2N30	#1	647.2	334.4	13.645	0.291	0.166	0.849	2.746	3	3
S4R2N32	#1	826.7	364.7	14.255	0.411	0.168	0.464	2.655	2	2
S4R2N33	#1	783.0	286.6	14.646	0.291	0.181	0.976	2.842	1	1
S4R2N34	#1	818.0	285.3	14.037	0.386	0.182	0.461	2.666	2	2
S4R3N2	#1	81.6	971.3	11.728	0.192	0.076	0.229	2.690	2	2
S4R3N20	#1	323.2	466.0	13.174	0.555	0.320	0.363	2.588	2	2
S4R3N23	#1	171.4	158.0	14.544	0.844	0.177	0.362	2.580	1	1
S4R3N24	#1	134.2	108.6	14.695	0.509	0.191	0.374	2.564	1	1

Table 6—Continued

Star	Frame	X Position	Y Position	V	b−y	m_1	c_1	β	N_{uvby}	N_β
S4R3N29	#1	602.6	138.9	12.782	0.493	0.140	0.434	2.615	2	2
S4R3N32	#1	654.2	297.3	-	-	-	-	2.690	-	1
S5000	#3	426.2	361.6	14.149	0.270	0.036	0.499	2.721	1	1
S5001	#3	859.1	309.1	15.116	0.565	0.157	0.274	2.557	1	1

Table 7. Unreddened indices and an estimation of the spectral classification for all the likely members of NGC 1893.

Star	$[c_1]$	$[m_1]$	[u−b]	T_{eff}	*SpectralType*	*Spectroscopic*
			O−Type			
S3R1N16	−0.111	0.030	−0.051	–	–	O8V(f)[1,2], O7V((f))[3,5]
S4R2N17	−0.176	0.063	−0.050	–	–	O6V(f)[1], O5[4]
S3R2N15	−0.107	0.061	0.016	–	–	O8[2], O6[3], O5V(f)[5]
			B−Type			
S2R2N43	−0.087	0.121	0.155	23710	B1	B1III[1], B0.5V[5]
S3R1N17	−0.126	0.145	0.164	23436	B1	B0.5V[1], B0.2V[5]
S3R2N18	0.071	0.058	0.188	22736	B1.5	B1.5V[1]
S2R2N41	−0.063	0.129	0.196	22512	B1.5	B1.5V[1,5]
S2R1N18	−0.086	0.168	0.249	21140	B2	B1V[1], B0.7V[5]
S3R1N1	0.099	0.079	0.257	20948	B2	B2.5V[1], B2V[5]
S2R1N25	0.076	0.124	0.324	19476	B2	
S2R1N2	0.015	0.156	0.327	19415	B2	B1V[5]
S2R2N42	0.091	0.152	0.394	18156	B3	
S4R2N18	0.179	0.109	0.397	18104	B3	
S4R3N2	0.191	0.137	0.465	16999	B4	B2V[3]

Table 7—Continued

Star	$[c_1]$	$[m_1]$	[u−b]	T_{eff}	*SpectralType*	*Spectroscopic*
S2R1N7	0.061	0.203	0.467	16969	B4	
S1R2N20	0.104	0.182	0.468	16954	B4	
S2R1N24	0.218	0.127	0.471	16909	B4	
S2R2N20	0.131	0.181	0.493	16585	B4	
S3R1N6	0.282	0.106	0.494	16571	B4	
S3R3N11	0.343	0.082	0.507	16387	B4	
S3R1N2	0.299	0.119	0.536	15991	B5	
S2R1N12	0.178	0.190	0.558	15704	B5	
S3R2N2	0.323	0.122	0.567	15590	B5	
S2R1N23	0.312	0.135	0.582	15404	B5	
S3R2N4	0.410	0.110	0.630	14840	B6	
S3R2N5	0.384	0.123	0.631	14829	B6	
S2R2N40	0.426	0.117	0.660	14510	B6	
S1R2N1	0.321	0.183	0.687	14226	B6	
S2R1N15	0.297	0.196	0.689	14206	B6	
S5000	0.445	0.122	0.690	14195	B7	
S3R1N13	0.588	0.077	0.742	13684	B8	
S3R1N8	0.516	0.119	0.754	13572	B8	
S1R1N10	0.527	0.123	0.772	13408	B8	
S3R2N9	0.538	0.125	0.788	13265	B8	

Table 7—Continued

Star	$[c_1]$	$[m_1]$	[u−b]	T_{eff}	*SpectralType*	*Spectroscopic*
S3R2N13	0.747	0.049	0.845	13784	B9	
S2R1N3	0.580	0.145	0.870	12585	B9	
S1R1N7	0.459	0.253	0.965	11888	B9	
S4R1N10	0.584	0.194	0.972	11840	B9	
S2R1N1	0.670	0.178	1.026	11485	B9	
S1R2N6	0.725	0.172	1.070	11213	B9	
			A−Type			
S2R2N25	0.781	0.259	1.299	10007	A0	
S4R1N16	0.879	0.232	1.343	9809	A0	
S1R1N4	0.908	0.237	1.382	9641	A1	
S2R3N59	0.994	0.212	1.417	9496	A1	

References. — [1]Massey et al. (1995); [2]Hoag et al. (1965); [3]Hiltner (1966); [4]Hiltner (1956); [5]This work

Table 8. Intrinsic photometric parameters for all the likely members of NGC 1893. The color excess $E(b-y)$ has been calculated by applying Crawford's (1978) procedure. The average cluster reddening has been used to derive the intrinsic photometric parameters. The absolute magnitude and distance modulus are calculated by using the calibration of Balona & Shobbrook (1984), based on the value of the β index.

Star	E(b−y)	V_0	$(b-y)_0$	c_0	$M_V(\beta)$	$V_0-M_V(\beta)$
S1R1N4	0.371	14.287	0.013	0.911	1.674	12.613
S1R1N7	0.280	13.233	-0.123	0.434	-0.216	13.449
S1R1N10	0.346	13.184	-0.050	0.517	-0.305	13.489
S1R2N1	0.365	12.804	-0.052	0.311	-0.529	13.333
S1R2N6	0.360	13.794	-0.017	0.722	0.475	13.319
S1R2N20	0.464	11.911	0.026	0.109	-1.874	13.784
S2R1N1	0.324	12.837	-0.058	0.658	-0.030	12.867
S2R1N2	0.316	10.728	-0.131	-0.011	-2.478	13.206
S2R1N3	0.328	13.106	-0.063	0.567	-0.148	13.254
S2R1N7	0.294	12.021	-0.148	0.031	-1.757	13.778
S2R1N12	0.335	11.284	-0.096	0.159	-1.292	12.576
S2R1N15	0.282	12.779	-0.137	0.270	-0.711	13.490
S2R1N18	0.288	9.773	-0.169	-0.120	-3.389	13.162
S2R1N23	0.338	12.285	-0.079	0.296	-1.276	13.561
S2R1N24	0.377	11.302	-0.050	0.208	-1.085	12.387
S2R1N25	0.344	11.628	-0.097	0.057	-2.127	13.755
S2R2N20	0.314	11.751	-0.121	0.107	-1.304	13.055
S2R2N25	0.298	13.983	-0.073	0.766	1.213	12.770
S2R2N40	0.398	12.406	-0.008	0.424	-1.057	13.463
S2R2N41	0.287	10.575	-0.167	-0.096	-3.034	13.609

Table 8—Continued

Star	E(b−y)	V_0	$(b-y)_0$	c_0	$M_V(\beta)$	$V_0-M_V(\beta)$
S2R2N42	0.295	10.963	-0.144	0.062	-1.869	12.832
S2R2N43	0.294	10.045	-0.163	-0.120	-3.593	13.638
S2R3N59	0.410	13.831	0.066	1.007	1.479	12.352
S3R1N1	0.366	10.849	-0.072	0.085	-2.585	13.434
S3R1N2	0.335	12.244	-0.084	0.282	-1.223	13.467
S3R1N4	0.376	12.528	-0.046	0.257	-3.771	16.299
S3R1N6	0.383	11.065	-0.037	0.275	-1.412	12.477
S3R1N8	0.351	12.318	-0.046	0.507	-0.690	13.008
S3R1N16	0.386	8.854	-0.073	-0.126	-4.405	13.258
S3R1N17	0.344	9.919	-0.117	-0.149	-3.767	13.686
S3R2N2	0.320	11.159	-0.096	0.304	-1.429	12.588
S3R2N4	0.360	12.110	-0.048	0.400	-1.089	13.199
S3R2N5	0.475	13.000	0.065	0.397	-0.795	13.795
S3R2N9	0.558	13.825	0.163	0.571	-0.162	13.987
S3R2N13	0.494	13.866	0.120	0.771	0.019	13.847
S3R2N15	0.549	8.742	0.090	-0.089	-4.289	13.030
S3R2N18	0.515	11.487	0.074	0.086	-2.308	13.795
S3R3N11	0.558	13.082	0.144	0.372	-1.526	14.608
S3R3N13	0.607	13.757	0.210	0.559	-0.095	13.852
S4R1N10	0.326	13.485	-0.065	0.571	0.740	12.745

Table 8—Continued

Star	E(b−y)	V_0	$(b-y)_0$	c_0	$M_V(\beta)$	$V_0-M_V(\beta)$
S4R1N16	0.316	14.099	-0.045	0.870	0.959	13.140
S4R2N17	0.402	7.617	-0.064	-0.189	-5.555	13.171
S4R2N18	0.354	10.877	-0.077	0.164	-1.802	12.679
S4R3N2	0.291	10.308	-0.138	0.163	-1.411	11.719
S5000	0.344	12.729	-0.060	0.433	-0.652	13.381

Table 9. Photometric intrinsic indices for stars which are likely to be pre-main-sequence members of NGC 1893.

Star	V_0	$(b-y)_0$	c_0
S1R2N23	13.924	0.325	0.231
S2R1N16	14.136	0.463	0.502
S2R1N26	13.966	0.494	0.342
S3R1N3	12.192	0.273	0.090
S4R2N14	14.062	0.188	0.308
S4R2N15	13.068	0.262	0.254
S5001	13.696	0.235	0.208